

# Dynamical geometry associated with the collision manifold in the circular restricted three-body problem

Joshua Fitzgerald\*<sup>1</sup> and Shane Ross†<sup>2</sup>

<sup>1</sup>Engineering Mechanics Program, Virginia Tech, USA

<sup>2</sup>Aerospace and Ocean Engineering, Virginia Tech, USA

## Abstract

In the circular restricted three-body problem, the linearized phase space structure about the Lagrange points controls dynamical transit at low energies because the geometry of the zero-velocity curve forces the particle to pass through neighborhoods surrounding the equilibria. At high energies, the zero-velocity curve disappears, so the Lagrange points no longer dominate the dynamics. Recent numerical research has revealed the existence of “arches of chaos” which dramatically affect the courses of high-energy solar system trajectories. We demonstrate through numerical and analytical techniques that the arches of chaos coincide with the finite-time stable and unstable manifolds to the singularities at the primaries. Under Levi-Civita regularization, the singularities can be viewed as collision manifolds and the finite-time stable and unstable manifolds can be viewed as approaching the collision manifolds asymptotically, which enables the use of linearization techniques. These linearization techniques, as well as numerical experiments, yield insight into the local geometry.

## 1 Introduction

Investigating the topological structures that underlie particle dynamics in higher-fidelity models such as the circular restricted three body problem (CR3BP) is a critical area of research in astrodynamics. Some of these structures and their implications for spacecraft transport are well-understood—one example is the manifold geometry emanating from the CR3BP Lagrange points that controls transit throughout the CR3BP at low energies [1]—whereas the identification and analysis of others is a topic of active study. For example, a recent study by Todorović et al., which applied the finite Lyapunov indicator (FLI) to solar system dynamics, has revealed the existence of “Arches of Chaos” stretching throughout phase space [2]. Initial conditions on either side of these structures diverge dramatically under the flow. In this work, we

demonstrate that the arches of chaos may be identified with the stable and unstable manifolds to the singularities in the CR3BP.

## 2 The Levi-Civita Regularization

The CR3BP Hamiltonian in the planar case is as follows [1]:

$$H_{\text{CR3BP}} = \frac{1}{2} (p_x^2 + p_y^2) - xp_y + yp_x - \frac{1-\mu}{r_1} - \frac{\mu}{r_2} \quad (1)$$

$r_i$  is the distance between the particle and the  $i$ th primary,  $i \in 1, 2$ , and  $\mu$  is the mass parameter. The Hamiltonian diverges as  $r_i \rightarrow 0$ , and so singularities are present at the locations of the primaries, creating challenges for numerical and analytical investigation in arbitrarily small neighborhoods about the two masses.

To resolve these difficulties, we utilize the Levi-Civita regularization, which reformulates the CR3BP in order to remove one of the singularities from the system. We assume that the singularity to be regularized is the singularity about  $m_2$ . Then, the Levi-Civita regularization recasts the phase space variables into the following form [3]:

$$\begin{aligned} x - 1 + \mu &= u_1^2 - u_2^2, \\ y &= 2u_1u_2, \\ p_x &= \frac{U_1u_1 - U_2u_2}{2|u|^2}, \\ p_y - 1 + \mu &= \frac{U_1u_2 + U_2u_1}{2|u|^2} \end{aligned} \quad (2)$$

with  $|u|^2 = u_1^2 + u_2^2$ . In addition, the standard time  $t$  is rescaled into the Levi-Civita time  $\tau$  according to the conversion equation

$$dt = |u|^2 d\tau. \quad (3)$$

Regularization recasts the singularity as a *collision manifold* [4] which is included within the Levi-Civita phase space. Regularization, in addition to its analytical value, also facilitates numerical investigation:

\*Email: joshfitz@vt.edu.

†Email: sdross@vt.edu.

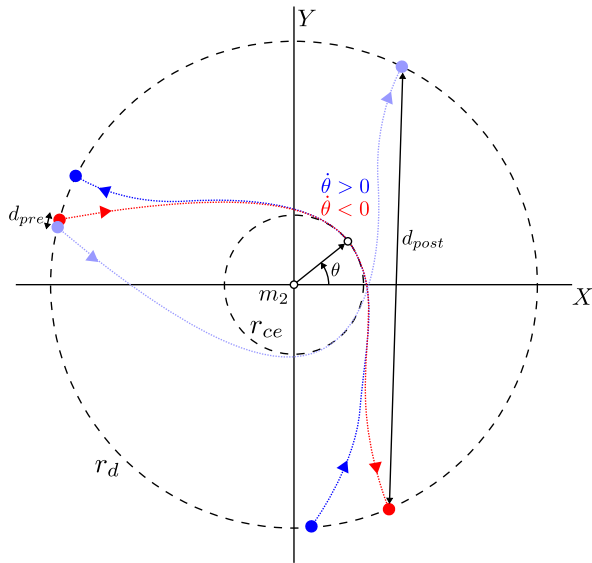


Figure 1: A schematic of the numerical experiment for examining how trajectories on either side of the stable manifold to the singularity move throughout phase space. The red and dark blue trajectories are generated at an initial radius  $r_{ce}$  but have  $\dot{\theta} < 0$  and  $\dot{\theta} > 0$ , respectively. They reflect one choice of  $\theta$ , but a whole family of trajectories for different values of  $\theta$  must be generated in order to match + and - pairs along the detection radius  $r_d$ . We integrate forwards and backwards and then match those + and - trajectories whose final position in backwards time was nearest to each other; in the schematic, the red - trajectory has been matched with a light blue + trajectory, generated in the same way as the dark blue trajectory for a different value of  $\theta$ . We then compare the pre-encounter, four-dimensional phase space distance  $d_{pre}$  with the post-encounter distance  $d_{post}$  for each matched pair.

attempting to integrate the standard CR3BP equations of motion in the vicinity of the singularity often causes the algorithm to fail as the step size becomes too small. Performing the procedure in the Levi-Civita equations of motion and then converting to and from standard form as required is a very efficient workaround.

### 3 Linearization of the Collision Manifold

The Hamiltonian for the system becomes

$$H_{LCR} = \frac{(U_1 + 2|u|^2 u_2)^2}{8} + \frac{(U_2 - 2|u|^2 u_1)^2}{8} - \frac{|u|^6}{2} - \mu - |u|^2 \left( E + \frac{(1-\mu)^2}{2} \right) - (1-\mu)|u|^2 \left( \frac{1}{\sqrt{1 + 2(u_1^2 - u_2^2) + |u|^4}} + u_1^2 - u_2^2 \right)$$

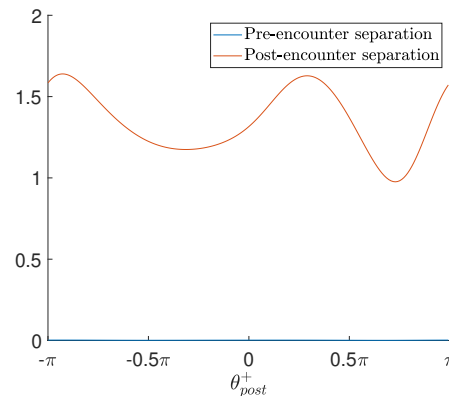


Figure 2: The + and - trajectories have an essentially constant, very small initial separation pre-encounter, but post-encounter their separation varies significantly depending on the angle along the detection circle (in this case, we use  $\theta_{post}^+$ , the post-encounter angle of each + trajectory, as the angle for identifying and sorting matched pairs of + and - trajectories).

where  $E$  is the  $H_{CR3BP}$  energy of the trajectory under consideration.  $H_{LCR}$  is defined at the collision manifold; although  $E$  diverges,  $|u|^2 = 0$ , and so the Hamiltonian overall does not diverge. Furthermore, the right-hand side of the equations of motion associated with this Hamiltonian is equal to zero at the collision manifold, and so the singularity becomes an equilibrium point under Levi-Civita regularization.

We demonstrate that linearizing this singularity reveals it to be a saddle  $\times$  saddle point in Levi-Civita space. Although the point itself is excised from the phase space when converted back to the standard CR3BP, the local geometry about the point is preserved, and so linearizing the collision manifold is key to understanding the dynamical geometry in standard form.

## 4 Sample Numerical Results

### 4.1 Quantifying divergence due to the manifolds

We investigate the collision manifold and its stable and unstable manifolds using numerical experiments in order to develop intuition regarding the nature of the system.

For example, consider only the stable manifolds for simplicity. In  $m_2$ -centered polar coordinates  $[r \ \theta \ \dot{r} \ \dot{\theta}]^T$ , initial conditions sufficiently close to the singularity along the stable manifolds have the form  $[r \ 0 \ \dot{r} \ 0]^T$  for  $0 < r \ll 1$  and  $\dot{r} \gg 1$ . One can consequently construct initial conditions on either side of the stable manifold that narrowly miss the singularity and whose local closest encounter distance to the singularity is given by  $r_{ce}$ . These initial conditions

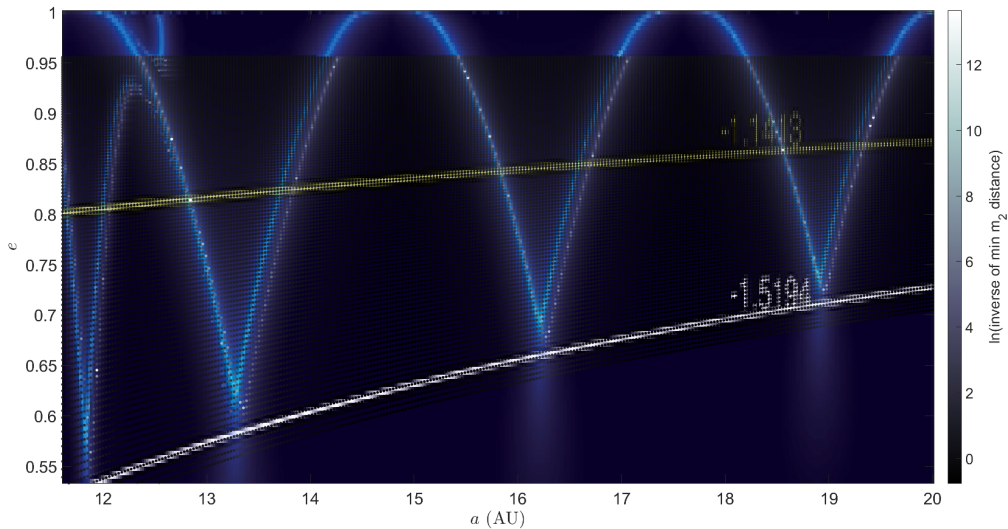


Figure 3: A portion of the semi-major axis/eccentricity plot of the Arches of Chaos given in [2], overlaid with the closest encounter distances of trajectories integrated within the basic CR3BP. The structures correspond almost exactly.

are given by  $[r_{ce} \ \theta \ 0 \ \pm\dot{\theta}]^T$  where  $\theta \in [-\pi, \pi)$ ,  $\dot{\theta}$  is chosen to target a desired energy, and the choice of  $\pm$  determines the side to which these initial conditions belong. For convenience, we call trajectories with positive  $\dot{\theta}$  “+ trajectories” and trajectories with negative  $\dot{\theta}$  “- trajectories.”

We integrate + and - trajectories forwards and backwards until they intercept a detection radius  $r_d \gg r_{ce}$  around  $m_2$  in both directions. + and - trajectories are matched into pairs based on which trajectories in each set had the closest pre-encounter angles along the detection radius with respect to each other. We then compare the pre-encounter distance  $d_{pre}$  and post-encounter distance  $d_{post}$  for each matched pair of + and - trajectories (see Figure 1). We discover that different intercept angles along the detection circle yield noticeably different post-encounter distances between + and - trajectories even though they start with the same extremely small pre-encounter distances (see Figure 2).

## 4.2 Replication of the arches

One very straightforward numerical experiment that demonstrates the connection between the stable and unstable manifolds to the singularities and the Arches of Chaos is to integrate grids of initial conditions and then to determine the minimum encounter distance of each trajectory to the singularity. By definition, trajectories with closer encounters to the singularity are closer to lying on the stable and unstable manifolds. By generating and plotting initial conditions in the same manner as in [2], the resultant structures can be compared (see Fig. 3).

## References

- [1] W. S. Koon, M. W. Lo, J. E. Marsden, S. D. Ross, *Dynamical Systems, the Three-Body Problem, and Space Mission Design*, Marsden Books, 2011.
- [2] N. Todorović, D. Wu, A. J. Rosengren, The arches of chaos in the solar system, *Science Advances* **6** (2020), eabd1313.
- [3] R. I. Paez, M. Guzzo, A study of temporary captures and collisions in the Circular Restricted Three-Body Problem with normalizations of the Levi-Civita Hamiltonian, *International Journal of Non-Linear Mechanics* **120** (2020), 103417.
- [4] J. Llibre, On the restricted three-body problem when the mass parameter is small, *Celestial mechanics* **28** (1982), 83-195.